EFFECTS OF HETEROGENEITY IN LITHOLOGY AND MECHANICAL PROPERTIES ON THE SLIP BEHAVIORS OF THE PLATE BOUNDARY FAULT AT THE HIKURANGI MARGIN, NEW ZEALAND

An Undergraduate Research Scholars Thesis

by

ALEXI ALLEN

Submitted to the Undergraduate Research Scholars program at
Texas A&M University
in partial fulfillment of the requirements for the designation as an

UNDERGRADUATE RESEARCH SCHOLAR

Approved by Research Advisor: Dr. Hiroko Kitajima

May 2020

Major: B.S. Geophysics

TABLE OF CONTENTS

ABSTRACT

Effects of heterogeneity in lithology and mechanical properties on the slip behaviors of the plate boundary fault at the Hikurangi margin, New Zealand

Alexi Allen
Department of Geology and Geophysics
Texas A&M University

Research Advisor: Dr. Hiroko Kitajima
Department of Geology and Geophysics
Texas A&M University

Subduction zones are known to produce large, damaging earthquakes, but they can also experience slow-slip events which cannot be felt by humans. Understanding the mechanisms which influence this variation in slip rate will allow us to better anticipate how the subduction zone will act in the future. While the seafloor sediments make up a small portion of the subducting oceanic plate, they can have a noticeable impact on its ability to produce both large earthquakes and slow-slip events. Cores containing sediments and basement rock recovered by the International Ocean Discovery Program (IODP) from the Hikurangi Subduction zone near New Zealand were scanned using X-ray fluorescence (XRF) to obtain their chemical composition. Using the XRF data with in-situ measurements of porosity, p-wave velocity, and drilling parameters, as well as lab tests to determine the strength of these rocks, we can evaluate how the composition of the sediments affects their physical properties. A strong correlation between calcium content, porosity, and p-wave velocity was seen for the volcaniclastic cores. There is also evidence to suggest that the torque on bit during drilling is an indication of rock strength as it changes sharply at certain lithologic boundaries. Triaxial compression tests in the

lab were used to quantify the rock strength of the volcaniclastic materials. This investigation into the subducting sediment properties builds onto pre-existing studies into the effects of seamounts on subduction and the factors that influence the slip rate at subduction zones.

ACKNOWLEDGMENTS

I would like to thank my faculty advisor, Dr. Kitajima for allowing me this opportunity and the patience and guidance necessary to make it happen. I would also like to thank Dan Brandenburg and Xiaofeng Chen who assisted me in the Handin Rock Deformation Lab and Dr. Brian LeVay for his help operating the XRF scanner at the IODP.

This thesis would not have been possible without the contributions made by the scientists aboard IODP Expedition 375 and the cores recovered during this expedition.

Thanks to my friends and family who have supported me during this process and encouraged me to finish my thesis.

NOMENCLATURE

TAMU	Texas A&M University
IODP	International Ocean Discovery Program (previously the Integrated Ocean Discovery Program)
MPa	Mega-Pascal
WOB	Weight on Bit (klb)
RPM	Rotations per Minute
TOB	Torque on Bit (klb×ft)
mbsf	Meters below seafloor
GR	Gamma ray

CHAPTER I

INTRODUCTION

Earthquakes are one of the most destructive events on the planet and not just from the shaking. Fires, tsunamis, and disease can also occur in the aftermath of earthquakes depending on the severity. This severity is determined by the rupture size and energy release of a fast-slip event. However, plates can also slip slowly and release the strain build-up in a less destructive manner. Fault zones that accommodate slow slip events can also generate large, damaging events. There is not a clear understanding of what mechanisms work within the fault zone to cause a slow or fast-slip event. At the Hikurangi margin off the eastern coast of the North Island of New Zealand, the slow slip events occur at relatively shallow depths so that it is easier to study slow-slip events by scientific ocean drilling (Barker et al., 2018). Increasing our understanding of why this subduction zone slips slowly will help us to better understand why large fast-slip events occur and better prepare for damaging events in the future.

The subducting material will be analyzed by two methods. First, obtaining XRF (X-ray Fluorescence) data allows us to determine the chemical composition of a core by irradiating the surface of the rock with X-rays (Cook et al., 1975). The energy given off by electrons jumping between the orbitals of specific atoms is recorded. Quantifying the energy released allows us to measure the amounts of certain elements within the rock core. Second, an analysis of drilling parameters can provide some mechanical properties (e.g., rock strength) of formation at depth, based on how easily the drill bit can progress with depth (Li & Itakura, 2012). Because the drilling parameters such as rotation speed, weight on bit, torque on bit, and penetration rate were recorded every second during the drilling operation, the analysis can characterize mechanical

properties of the complete sections of the formation at depth (Hamada et al., 2018). The best way to obtain a complete understanding of the rock strength is to compare this drilling data with lab testing.

The purpose of this study is to determine how heterogeneities in the composition and mechanical properties of seafloor sediments impact slow slip mechanics at the Hikurangi subduction zone off the coast of New Zealand. This study will help us better understand what affects how quickly a fault slips and will allow us to better understand the mechanisms responsible for many of Earth's most devastating seismic events. Previous research has been conducted on the effects of fluid pressure and subducting seamounts on the slip behaviors of subduction plate boundary faults (Bell et al., 2010). This study will build upon these previous experiments by comparing the chemical composition of the sediments to the strength of the rocks obtained from lab tests and interpreted from drilling data. As the top layer of the subduction crust, seafloor sediments are likely to play a role in the ability of the lower plate to subduct (Rabinowitz et al., 2018). I have characterized these effects and quantified them through a combination of XRF, drilling parameter analysis, and laboratory experiments at elevated pressure.

CHAPTER II

METHODS

Geological Setting of the Hikurangi Margin

The Pacific plate subducts beneath the Australian plate at a rate of about 5 cm/year along the east coast of the North Island of New Zealand to form the Hikurangi margin (Figure 1) (Wallace et al., 2004). This subducting plate contains the Hikurangi Plateau, a large igneous province created in the Cretaceous which is overlain by ~1 km thick layer of sediment which increases to a thickness of >5 km to the south. The margin is generally non-accretionary, but in the northern part of the margin, the subduction is characterized by a largely deformed accretionary wedge overlying less deformed, subducting rocks. This margin in this region is known to experience slow slip events (SSEs) once every 18-24 months resulting in a displacement of 1-3 cm southward (Wallace and Beavan, 2010; Wallace et al., 2016). These SSEs are hypothesized to originate from a layer of under-compacted, highly pressurized sediments along the décollement where fluid pressure may reduce the effective stress and encourage smooth sliding (Figure 2). The International Ocean Discovery Program (IODP) Expeditions 372/375 have drilled along a transect in that region off the northeastern coast of New Zealand, and collected ocean sub-seafloor cores and logging data (Figure 1). This study focuses on the two drilling sites, Sites U1520 and U1526, to understand how the different lithologies of rocks composing the subducting plate affect its physical and mechanical properties. Site U1520 is located on the floor of the Hikurangi Trough between the deformation front and Turanganui Knoll. Site U1526 is located on the western flank of the Turanganui Knoll seamount (Figures 1 and 2). At Site U1520, multiple holes were drilled for logging and coring operations;

logging-while-drilling (LWD) was conducted in Holes U1520A and U1520B (Figure 3). Hole U1520C was first drilled and cased to 646 meters and cored from 646 to 1054 mbsf. Hole U1520D was drilled for coring from the shallower portions of the seafloor to 642 mbsf. Different lithologies were observed at Site U1520 including hemipelagic facies (lithostratigraphic Units I-III; 0-510 mbsf), pelagic facies (lithostratigraphic Unit IV; 510-848 mbsf), volcaniclastic facies (lithostratigraphic Unit V; 848-1016 mbsf), and mixed faces (lithostratigraphic Unit VI; 1016-1054 mbsf) (Figure 4). This study mainly uses the data from the deeper portion of Holes U1520B and U1520C. At Site U1526, holes U1526A and U1526B were drilled only for coring. This study uses the cores from Hole U1526A.

Chemical Data

The cores recovered during IODP Expedition 375 were split into working and archive halves on the ship during the expedition and have been stored in the IODP Gulf Coast Repository on the TAMU campus. Selected cores from Sites U1518, U1520 and U1526 were scanned using the XRF machine at the repository to determine their chemical composition. The data collected from cores at Sites U1520 and U1526 were used for this study. The working faces of the archive core halves were scraped with a microscope slide to flatten the surface and remove any fungus that had grown while in cold storage. This was more readily accomplished on the soft sediment cores predominantly from Site U1520 than the cores from Site U1526 where the basaltic seamount was located (Figures 1 and 2). For the hard rock samples that could not be scraped, the pieces were leveled in the sleeve to prevent damage to the scanning mechanism. The cores were then covered with plastic wrap to prevent the film on the scanner from breaking. The argon intensity value was used as a quality control for the XRF data because it would record as positive if the scanner landed unevenly or on top of a crack detecting an air pocket. The data of calcium

and other elemental readings were then reduced and correlated to in-situ readings of physical properties taken during the drilling process such as porosity, P-wave velocity, gamma-ray attenuation bulk density, and magnetic susceptibility.

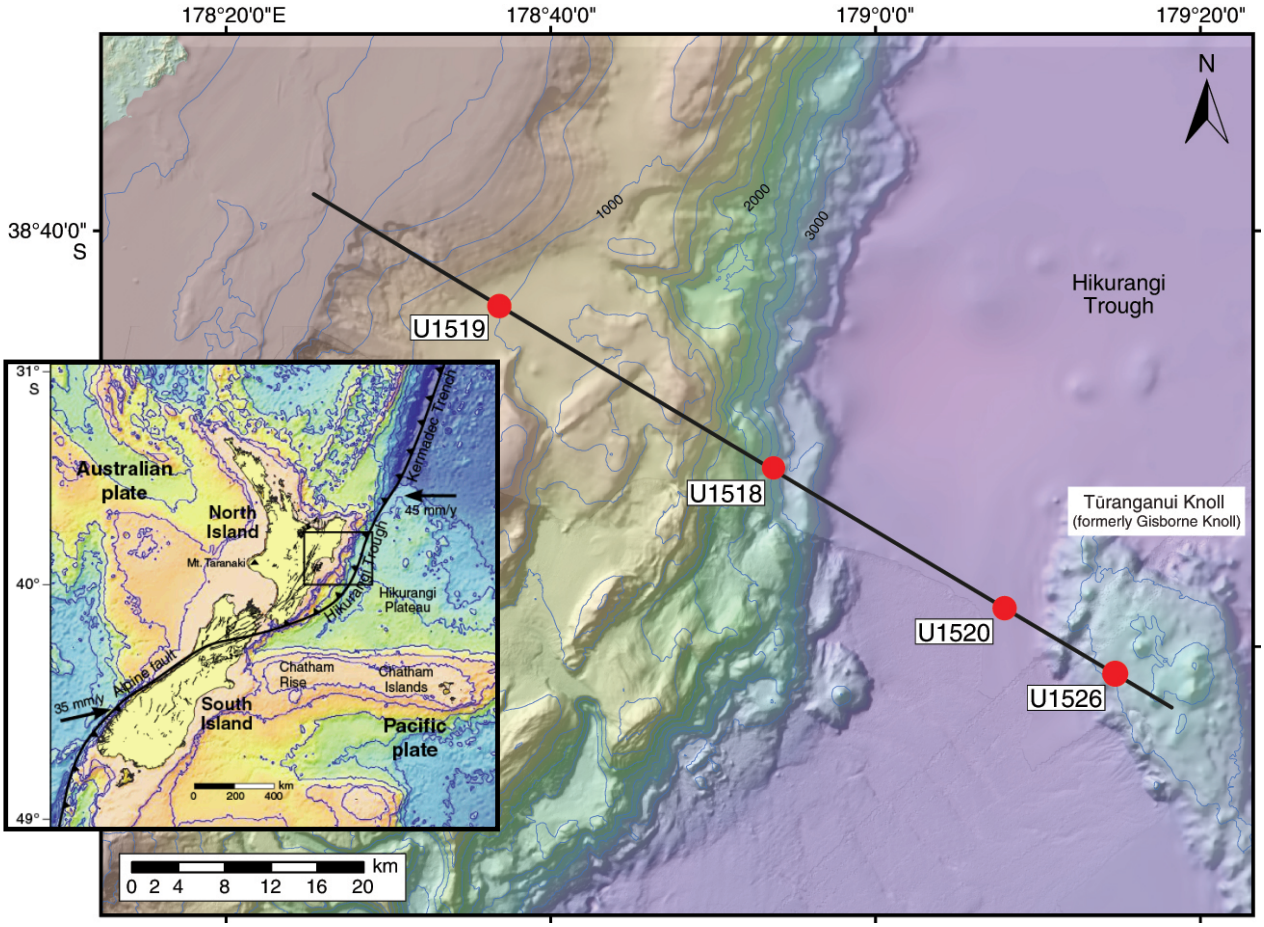

Figure 1. The transect of the sites drilled during Expedition 375 with bathymetry data shown (Wallace et al., 2019). New Zealand's North Island is located ~1° to the west of Sites U1520 and U1526 as shown in the inset map on the left. Site U1520 was drilled into seafloor sediments; whereas, Site U1526 was drilled into the nearby basaltic knoll.

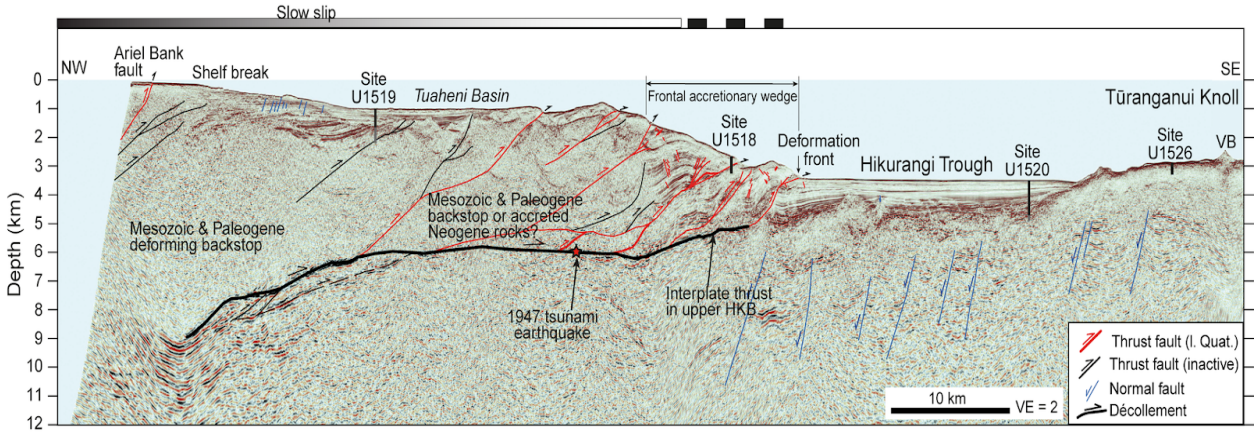

Figure 2. A seismic profile of the drilled area with the cored locations and depths marked (Wallace et al., 2019). Site U1520 is composed of hemipelagic and pelagic sediments overlying the volcaniclastic rocks. Site U1526 is composed of fresh basalt and both sites are located on the subducting plate.

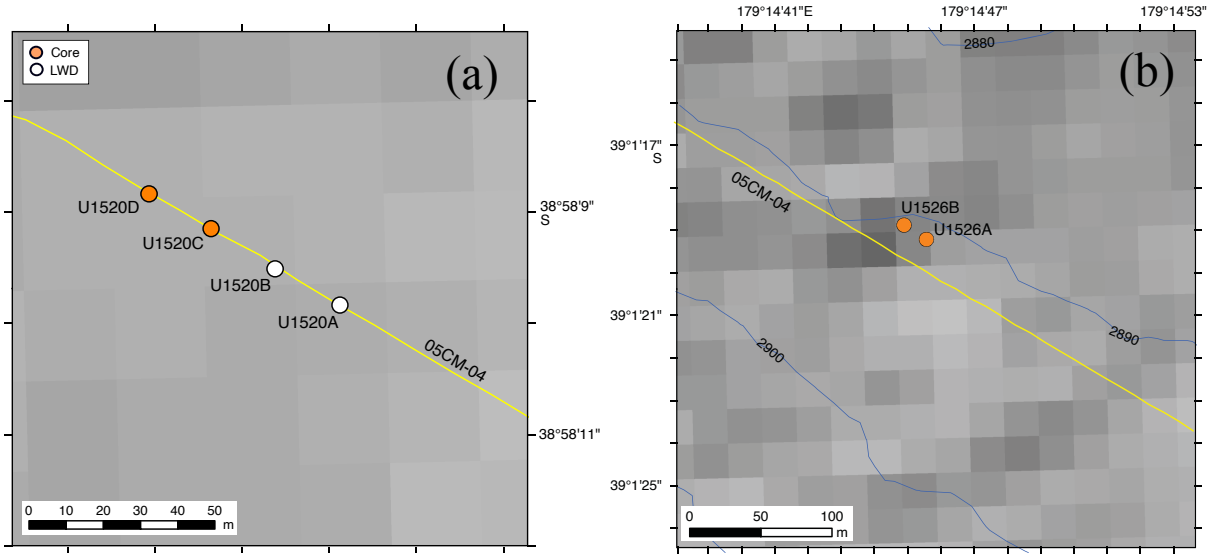

Figure 3. Zoomed images of the drilling transect at (a) Site U1520 and (b) Site U1526 showing the locations of the drilled holes from which cores were recovered.

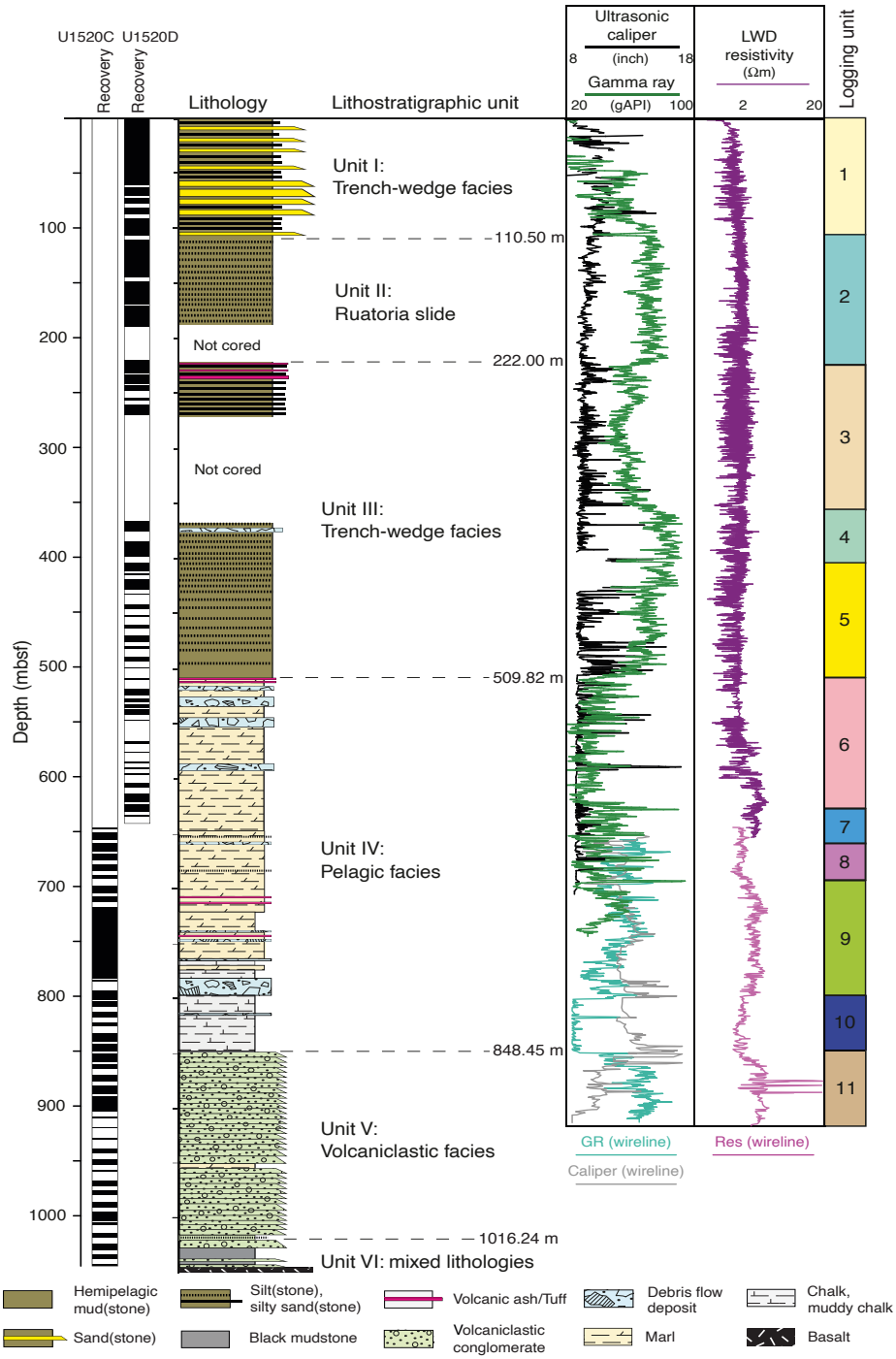

Figure 4. Lithostratigraphic summary for Site U1520. Black indicates where core was recovered; white is no recovery. Logging units, logging-while-drilling (LWD) measurements from Hole U1520B, and wireline logging results from Hole U1520C are also shown (Barnes et al., 2019).

Drilling Data

The data collected from Site U1520 were used for the drilling parameter analysis. The data from the deeper portion (657.5-1065 mbsf) of Hole U1520C at Site U1520 was analyzed in this study. The data were recorded every second and include the weight on the drilling bit (WOB), torque on bit (TOB), rotations per minute (RPM), and the bit depth. The original data contained many instances where the WOB dropped to zero due to core recovery and pipe connection every ~10 m advance. WOB defines how much force is acting on the bit as it drills into the rock. Therefore, zero WOB corresponds to the time while the drill is not proceeding. Thus, all the data points where the weight on bit was not positive were removed from the data. Then, a moving average over a 100 second window was applied to the data to smooth the noise. Lastly, to prevent the bit from catching and stalling due to the ship heaves and drilling operations, the drilling bit was shifted up and down. This upwards motion caused repeated depth values to occur in the data and times where the bit was not proceeding or cutting the formation. The data where the bit was not proceeding were thus discarded to obtain only the data that correspond to the formation strength. The rate of penetration was calculated at each depth by dividing the change in bit depth by the incremental time. Other properties, such as bulk density and magnetic susceptibility, were also obtained from the shipboard measurements during the IODP Expedition 375 (Barnes et al., 2019). The data reduction and graph-making were done in MATLAB.

Strength Tests

Deformation experiments were conducted in the modified various strain rig (MVSR) of the Handin Rock Deformation Lab in the Department of Geology & Geophysics and Center for Tectonophysics (Chester, 1989; Kitajima et al., 2012). Triaxial compression strength tests were performed on 2 cylindrical samples prepared from the core (375-U1520C-34R-1, 0-11cm)

recovered from 948.5 mbsf at Site U1520, which is composed of volcaniclastic rock (Table 1). Although samples from the chalk section between 820 and 860 mbsf were planned to be tested, the deformation experiments were not able to be conducted due to COVID-19. Each sample was placed between the upper piston and a lower spacer and was jacketed with double layers of polyolefin to isolate the sample from the confining pressure medium of silicone oil. The two triaxial compression tests were run at a constant confining pressure of 1 MPa and 8.5 MPa and a constant axial displacement rate of 0.60 μm/s (equivalent strain rate of ~2.1×10^{-5} 1/s).

Table 1. Summary of samples from the triaxial deformation tests.

Experiment Number	**Sample**	**Length (mm)**	**Diameter (mm)**	**Mass (g)**	**Confining Pressure (MPa)**
AA2274	375-U1520C-34R-1 #2	28.55	12.17	6.9259	1
AA2273	375-U1520C-34R-1 #3	28.98	11.91	6.6886	8.5

CHAPTER III

RESULTS

Chemical Data

XRF element data and other physical properties show some correlations. Porosity decreases and P-wave velocity increases with calcium for the volcaniclastic samples from Site U1520 (Figure 5). The trends are not as apparent in the pelagic cores from Site U1520 or the basalt from Site U1526. The correlations observed in the volcaniclastic sections likely reflect the extent of calcium cementation. Cementation of calcium can fill the voids in the rock to decrease the porosity (Figure 5a) and increase the elastic property (i.e., P-wave velocity) (Figure 5b). A meaningful correlation between calcium and these properties is not seen for the pelagic cores because they are comprised mostly of carbonates. However, we do see a negative correlation between porosity and P-wave velocity for all of the units in Figure 6. This is to be expected since void space in a rock decreases its density (Figure 7a). As for magnetic susceptibility, the basaltic unit of Site U1526 shows the highest values, and the volcanic clastic unit shows the second highest values; however, neither unit shows clear correlation between magnetic susceptibility and calcium intensity (Figure 7b). The pelagic unit, on the other hand, shows a negative correlation; magnetic susceptibility decreases with increasing calcium intensity. This probably reflects the lithological transitions in the unit between calcareous mudstone, mark, and chalk. This data was also plotted against depth for Site U1520 with the boundary between the pelagic and volcaniclastic units highlighted (Figure 8). At this boundary, the P-wave velocity drops sharply. This could be due to some degree of disaggregation at the lithologic boundary of the volcaniclastic rocks; however, it is more likely that when the hole diameter caliper readings at

this interface increased, the P-wave travelled through the drilling fluid rather than the formation. The other properties, which were obtained for the cores that were scanned at the IODP, rather than obtained from LWD measurements, are not shown on this graph. Representative core images for the pelagic and volcaniclastic from Site U1520 and the basalt from Site U1526 are provided as Figures A2, A3 and A4 in the Appendix.

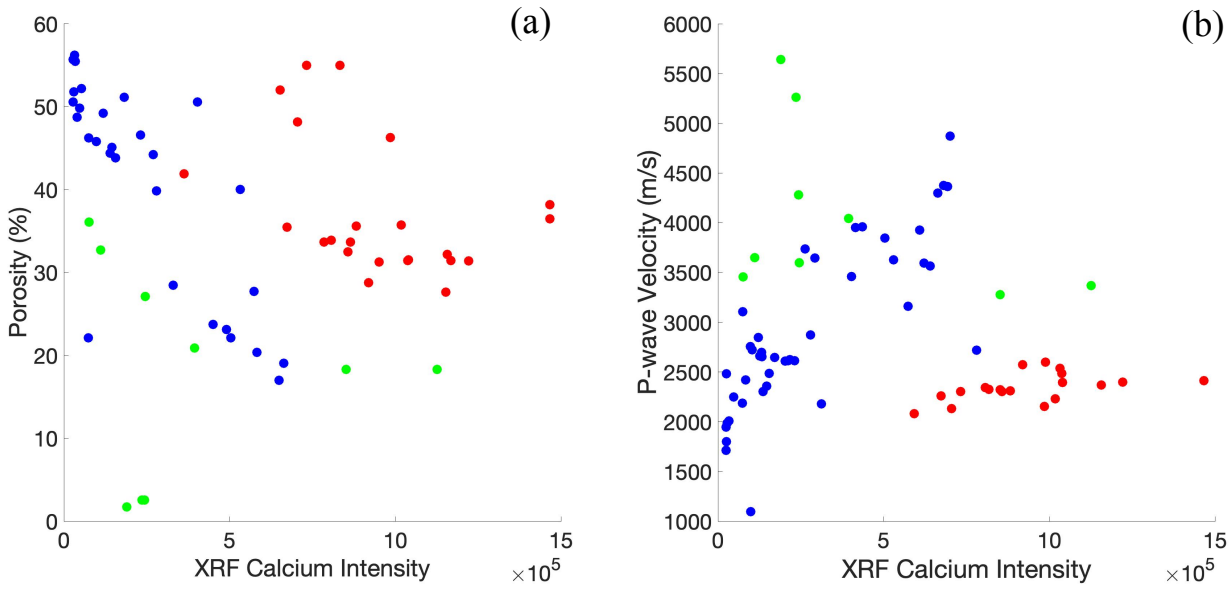

Figure 5. Correlation plots between (a) porosity and XRF calcium intensity and (b) P-wave velocity and XRF calcium intensity. The red symbols represent the pelagic unit at Site U1520; the blue symbols represent the volcaniclastic unit at Site U1520; and the green symbols represent the basalt at Site U1526.

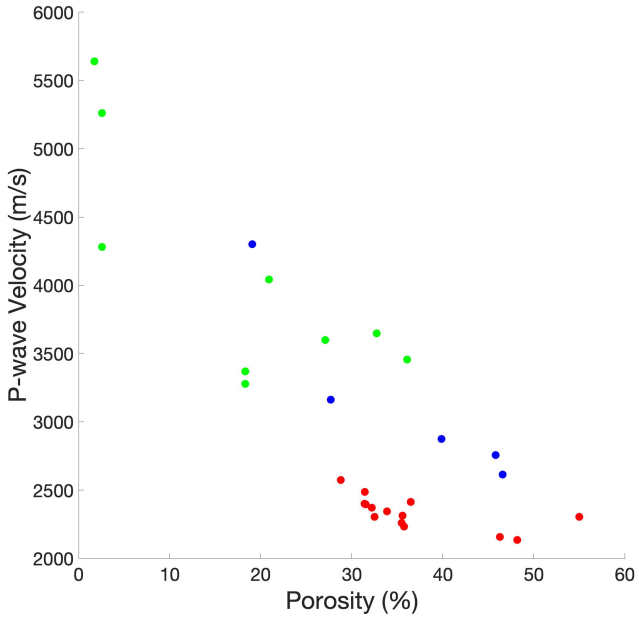

Figure 6. Correlation plot between P-wave velocity and porosity. The red symbols represent the pelagic unit at Site U1520; the blue symbols represent the volcaniclastic unit at Site U1520; and the green symbols represent the basalt at Site U1526.

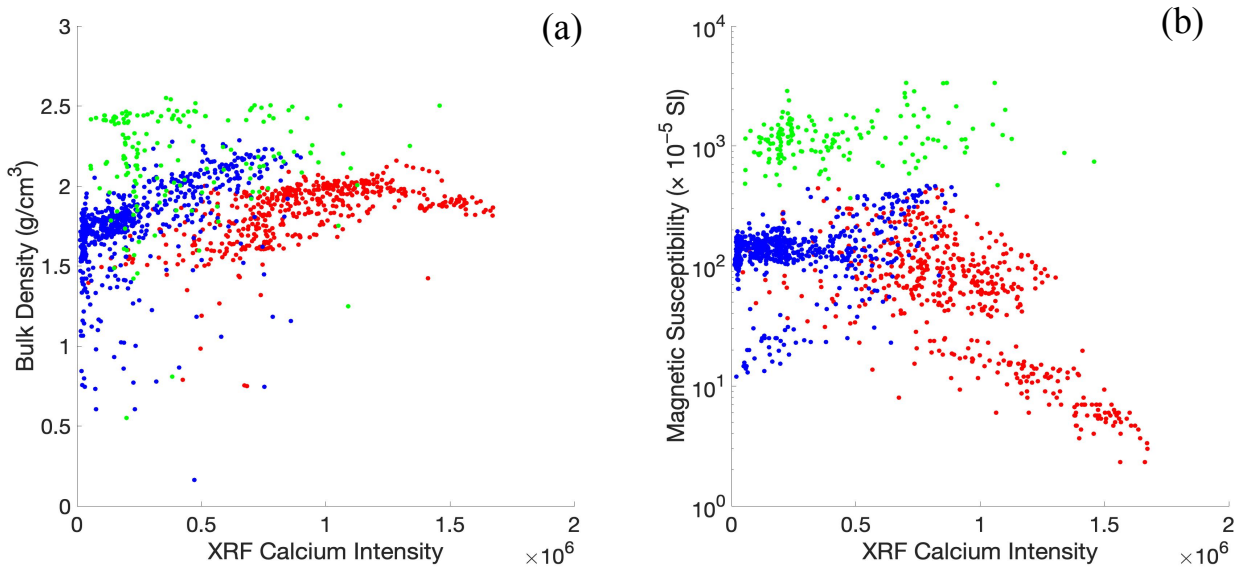

Figure 7. Correlation plots between (a) gamma ray attenuation bulk density and XRF calcium intensity and (b) magnetic susceptibility and XRF calcium intensity. The red symbols represent the pelagic unit at Site U1520; the blue symbols represent the volcaniclastic unit at Site U1520; and the green symbols represent the basalt at Site U1526.

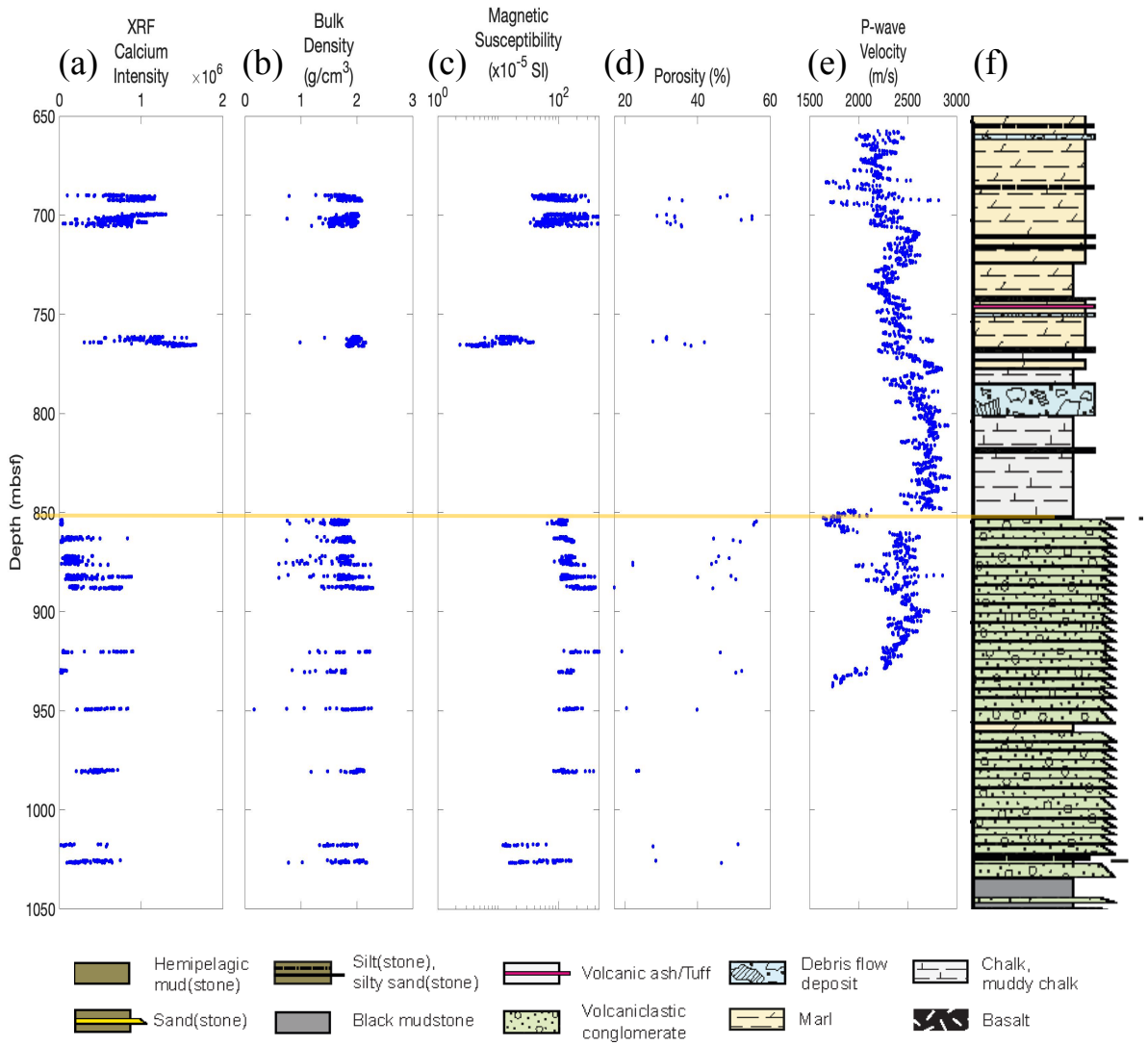

Figure 8. Depth-series data of physical properties of (a) XRF calcium intensity, (b) bulk density, (c) magnetic susceptibility, (d) porosity, and (e) P-wave velocity. Panel (f) shows the corresponding stratigraphic column for this section (Wallace et al., 2019). The yellow line indicates the boundary between the upper, pelagic unit and the lower, volcaniclastic unit at Site U1520.

Drilling Data

The analyzed drilling data are shown in time-based plots (Figure A1) and depth-based plots (Figure 13). By only selecting the positive WOB values in panel (d), the upper trend in the TOB (around 10 klb×ft) and RPM (around 50 rpm) was selected. This selection was then averaged to obtain less noise when plotted against depth. The RPM and TOB are less noisy in the pelagic sediments than in the volcaniclastic rock. This is most likely due to the increased heterogeneity of the volcaniclastic materials which would make the torque vary more than carbonate rocks. This difference in heterogeneity between the pelagic and volcaniclastic cores from Site U1520 is readily apparent in the core images in Figures A2 and A3. While the pelagic sediments are not uniform, there are a lot more clasts with varying lithology present and also different degrees of cementation in the volcaniclastic cores. There was also a sharp increase in the penetration rate and the WOB as the bit entered a chalk unit between ~810 and 860 mbsf. This would make sense if the bit encountered less resistance in this unit than the overlying marl shown in the stratigraphic column in Figure 13 (e). A similar jump in TOB and RPM can be seen at other lithologic boundaries as well. Since relating physical properties of the rocks with mechanical properties obtained from drilling were of interest in this study, P-wave velocity for the pelagic and volcaniclastic rocks from Site U1520 were plotted and a general increase in torque from one lithology to the next is observed (Figure 14).

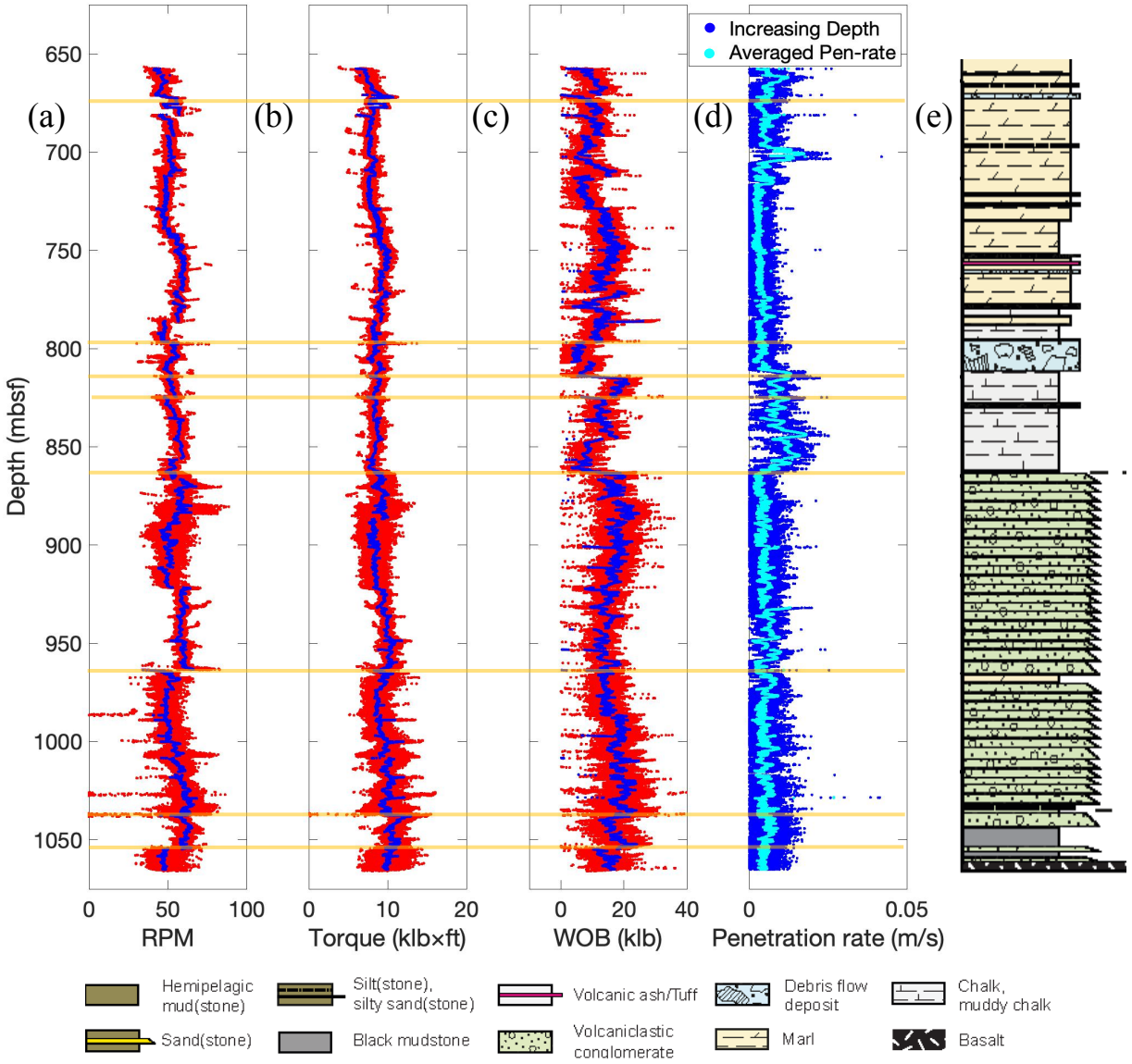

Figure 13. Depth-series data of drilling parameters of (a) rotation speed, (b) torque, (c) weight on bit, (d) penetration rate. The red points represent drilling data corresponding to only the depths with a positive WOB. The blue points represent the moving average data in Figure 12 when the depth was increasing between points; the cyan represents the penetration rate averaged over 100 seconds. Panel (e) shows the corresponding stratigraphic column for this section (Wallace et al., 2019). The yellow lines indicate jumps in the RPM, TOB, and penetration rate that correspond to lithologic boundaries.

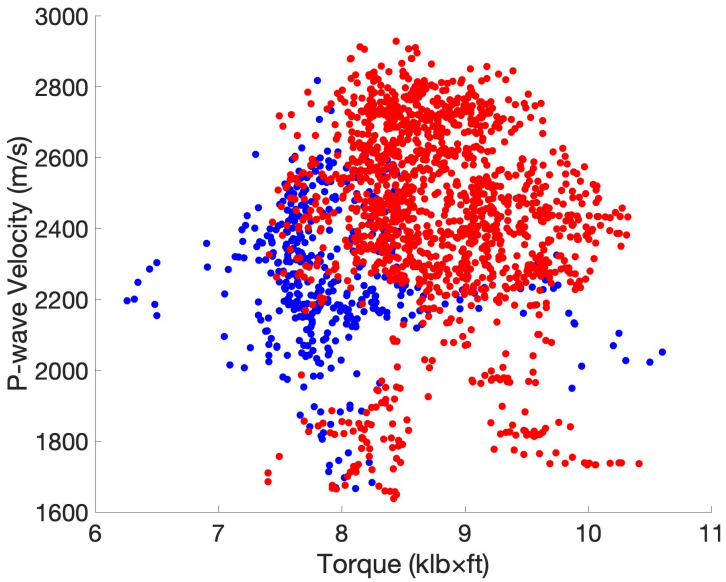

Figure 14. Correlation plot between torque and P-wave velocity. The blue is the pelagic unit and the red is the volcaniclastic unit both at Site U1520.

Strength Tests

Stress-strain curves (Figure 15) generated from the triaxial compression experiments show how the strength of the volcaniclastic rock from Site U1520 changes with different confining pressures of 1 MPa and 8.5 MPa. Confining pressure of 8.5 MPa is equivalent to the in-situ effective overburden stress at the sample depth (~650 mbsf) at Site U1520. The confining pressure of 1 MPa was chosen to correlate the fracture strength to the drilling parameter analysis. The volcaniclastic rock deformed at 1 MPa exhibits brittle deformation. The strength reaches a peak strength of 19.8 MPa followed by a stress drop to reach a residual strength of ~11.2 MPa. The sample deformed at 8.5 MPa, on the other hand, exhibits transitional and more ductile deformation; the strength reaches 43.4 MPa and gradually decreases to 39.5 MPa before the experiment was stopped. The Young's modulus for the 1 MPa confining pressure sample was ~1.08 GPa and ~1.65 GPa for the 8.5 MPa sample.

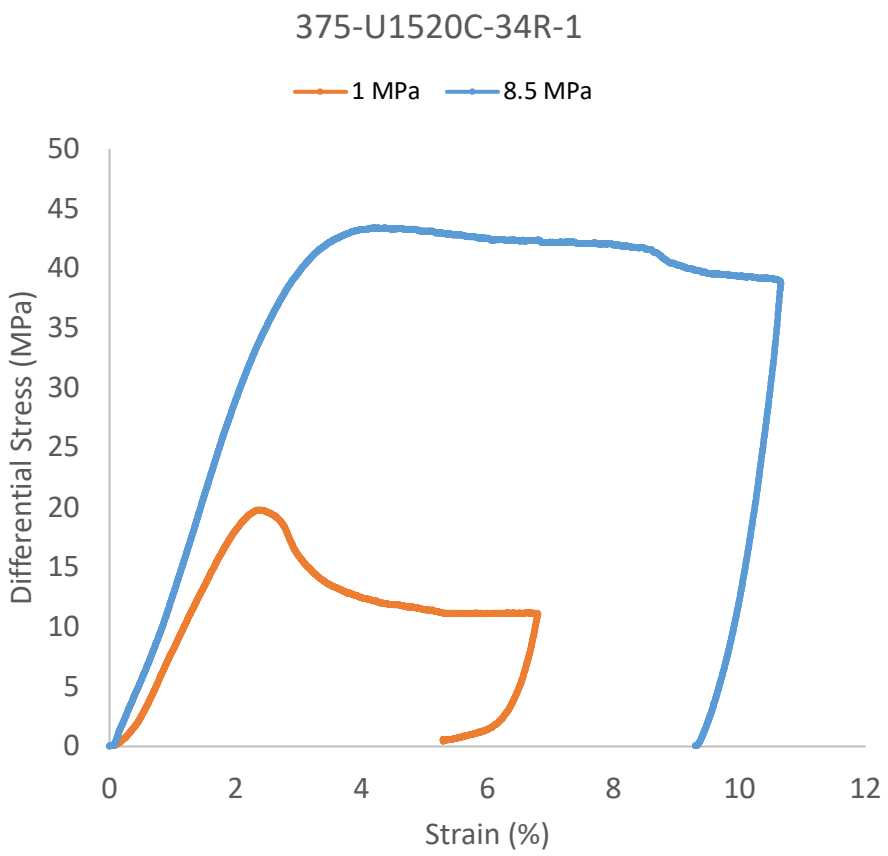

Figure 15. Stress-strain curves of two triaxial compression tests on the Sample 375-U1520C-34R-1 at confining pressure of 1 MPa (orange) and 8.5 MPa (blue). The sample deformed at 1 MPa exhibits brittle deformation after reaching the peak strength of 19.8 MPa; whereas, the sample deformed subjected to the higher confining pressure at 8.5 MPa exhibits a more ductile deformation after its peak stress at 43.4 MPa.

CHAPTER IV

CONCLUSION

This work was meant to investigate the relationship between chemical, physical and mechanical properties of rocks entering the Hikurangi subduction zone by integrating X-ray fluorescence scanning of cores, triaxial deformation experiments, and drilling parameter analysis. The positive correlation between calcium, bulk density, and P-wave velocity is observed in the volcaniclastic cores from Site U1520 due to precipitation within the pore spaces of the rock. The volcaniclastic rocks, which overall had a higher P-wave velocity than the pelagic cores, also indicate a higher torque in the drilling parameters. The triaxial deformation experiments of the volcaniclastic unit result in brittle deformation at 1 MPa, and transitional and more ductile behavior at 8.5 MPa.

Unfortunately, due to complications resulting from the shelter-in-place measures implemented by Brazos County and Texas A&M University against COVID-19, not all of the planned data collection for this paper was completed by the URS Thesis Program deadline. Deformation experiments on the samples from the chalk section between 820 and 860 mbsf were planned and prepared, but the actual experiments were not conducted. Nonetheless, the effects of lithology on the chemical, physical and mechanical data, are visible in the correlations across the different datasets. This study can be expanded in the future to include deformation experiments on the pelagic units and the use of laboratory data to calibrate the drilling parameter analysis to estimate the formation strength at depth.

REFERENCES

Barker, D. H. N., Henrys, S., Tontini, F. C., Barnes, P. M., Bassett, D., Todd, E., & Wallace, L. (2018). Geophysical constraints on the relationship between seamount subduction, slow slip, and tremor at the north Hikurangi subduction zone, New Zealand. *Geophysical Research Letters*, 45(23), 12,804 – 12,813. https://doi.org/10.1029/2018GL080259

Barnes, P.M., Wallace, L. M., Saffer, D. M., Pecher, I.A., Petronotis, K. E., Levay, L. J., Bell, R. E., Crundwell, M. P., Engelmann de Oliveira, C. H., Fagereng, A., Fulton, P. M., Greve, A., Harris, R. N., Hashimoto, Y., Hüpers, A., Ikari, M. J., Ito, Y., Kitajima, H., Kutterolf, S., Lee, H., Li, X., Luo, M., Malie, P. R., Meneghini, F., Morgan, J. K., Noda, A., Rabinowitz, H. S., Savage, H. M., Shepherd, C. L., Shreedharan, S., Solomon, E. A., Underwood, M. B., Wang, M., Woodhouse, A. D., Bourlange, S. M., Brunet, M. M. Y., Cardona, S., Clennell, M. B., Cook, A. E., Dugan, B., Elger, J., Gamboa, D., Georgiopoulou, A., Han, S., Heeschen, K. U., Hu, G., Kim, G. Y., Koge, H., Machado, K. S., McNamara, D. D., Moore, G. F., Mountjoy, J. J., Nole, M. A., Owari, S., Paganoni, M., Rose, P. S., Screaton, E. J., Shankar, U., Torres, M. E., Wang, X., & Wu, H.-Y. (2019). Site U1520. *In* Wallace, L.M., Saffer, D.M., Barnes, P.M., Pecher, I.A., Petronotis, K.E., LeVay, L.J., and the Expedition 372/375 Scientists, *Hikurangi Subduction Margin Coring, Logging, and Observatories.* Proceedings of the International Ocean Discovery Program, 372B/375: College Station, TX (International Ocean Discovery Program). https://doi.org/10.14379/iodp.proc.372B375.105.2019

Chester, F. M. (1989), Dynamic recrystallization in semi-brittle faults, *Journal of Structural Geology*, 11(7), 847–858, doi:10.1016/0191- 8141(89)90102-8

Cook, H.E., Johnson, P.D., Matti, J.C., & Zemmels, I. (1975) Methods of sample preparation and X-ray diffraction data analysis, X-ray Mineralogy Laboratory, Deep Sea Drilling Project, University of California, Riverside. https://doi.org/10.2973/dsdp.proc.28.app4.1975

Hamada, Y., Kitamura, M., Yamada, Y., Sanada, Y., Sugihara, T., Saito, S., Moe, K., & Hirose, T. (2018). Continuous depth profile of the rock strength in the Nankai accretionary prism based on drilling performance parameters. *Sci Rep*, 8(1)**,** 2622 https://doi.org/10.1038/s41598-018-20870-8

Kitajima, H., Chester, F. M., and Biscontin, G. (2012), Mechanical and hydraulic properties of Nankai accretionary prism sediments: Effect of stress path, *Geochem. Geophys. Geosyst.*, 13, Q0AD27, doi:10.1029/2012GC004124

Li Z., & Itakura, K. (2012). An analytical drilling model of drag bits for evaluation of rock strength. *Soils and Foundations*, 52(2), 216-227. https://doi.org/10.1016/j.sandf.2012.02.002.

Rabinowitz, H. S., Savage, H. M., Skarbek, R. M., Ikari, M. J., Carpenter, B. M., & Collettini, C. (2018). Frictional behavior of input sediments to the Hikurangi Trench, New Zealand. *Geochemistry, Geophysics, Geosystems*, 19(9), 2973– 2990. https://doi.org/10.1029/2018GC007633

Wallace, L. M., and Beavan, J. (2010), Diverse slow slip behavior at the Hikurangi subduction margin, New Zealand, *J. Geophys. Res.*, 115, B12402, doi:10.1029/2010JB007717.

Wallace, L. M., Beavan, J., McCaffrey, R., and Darby, D. (2004), Subduction zone coupling and tectonic block rotations in the North Island, New Zealand, *J. Geophys. Res.*, 109, B12406, doi:10.1029/2004JB003241.

Wallace, L. M., Saffer, D. M., Barnes, P. M., Pecher, I. A., Petronotis, K. E., LeVay, L. J., & the Expedition 372/375 Scientists (2019). Hikurangi subduction margin coring, logging, and observatories. Proceedings of the International Ocean Discovery Program, 372B/375: College Station, TX (International Ocean Discovery Program). https://doi.org/10.14379/iodp.proc.372B375.2019.

Wallace, L. M., Webb, S. C., Ito, Y., Mochizuki, K., Hino, R., Henrys, S., et al. (2016). Slow slip near the trench at the Hikurangi subduction zone, New Zealand. *Science*, 352(6286), 701– 704. https://doi.org/10.1126/science.aaf2349.

APPENDIX A

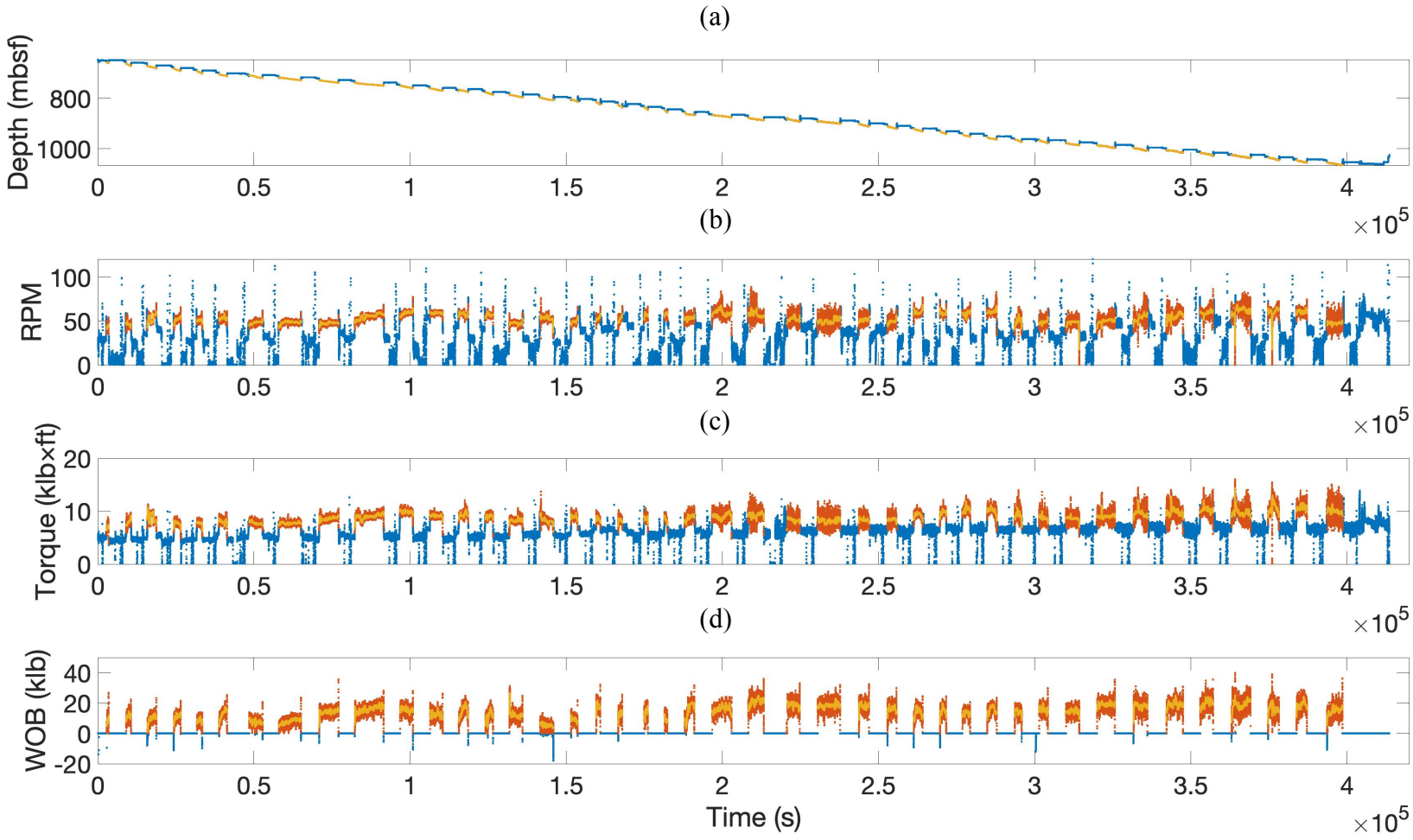

Figure A1. Time-series data of drilling parameters of (a) bit depth, (b) rotation speed (rpm), (c) torque on bit, (d) weight on bit (WOB). The blue dots represent the raw data, the orange dots represent the data with a positive WOB, the yellow dots represent the moving average data over a 100 window seconds.

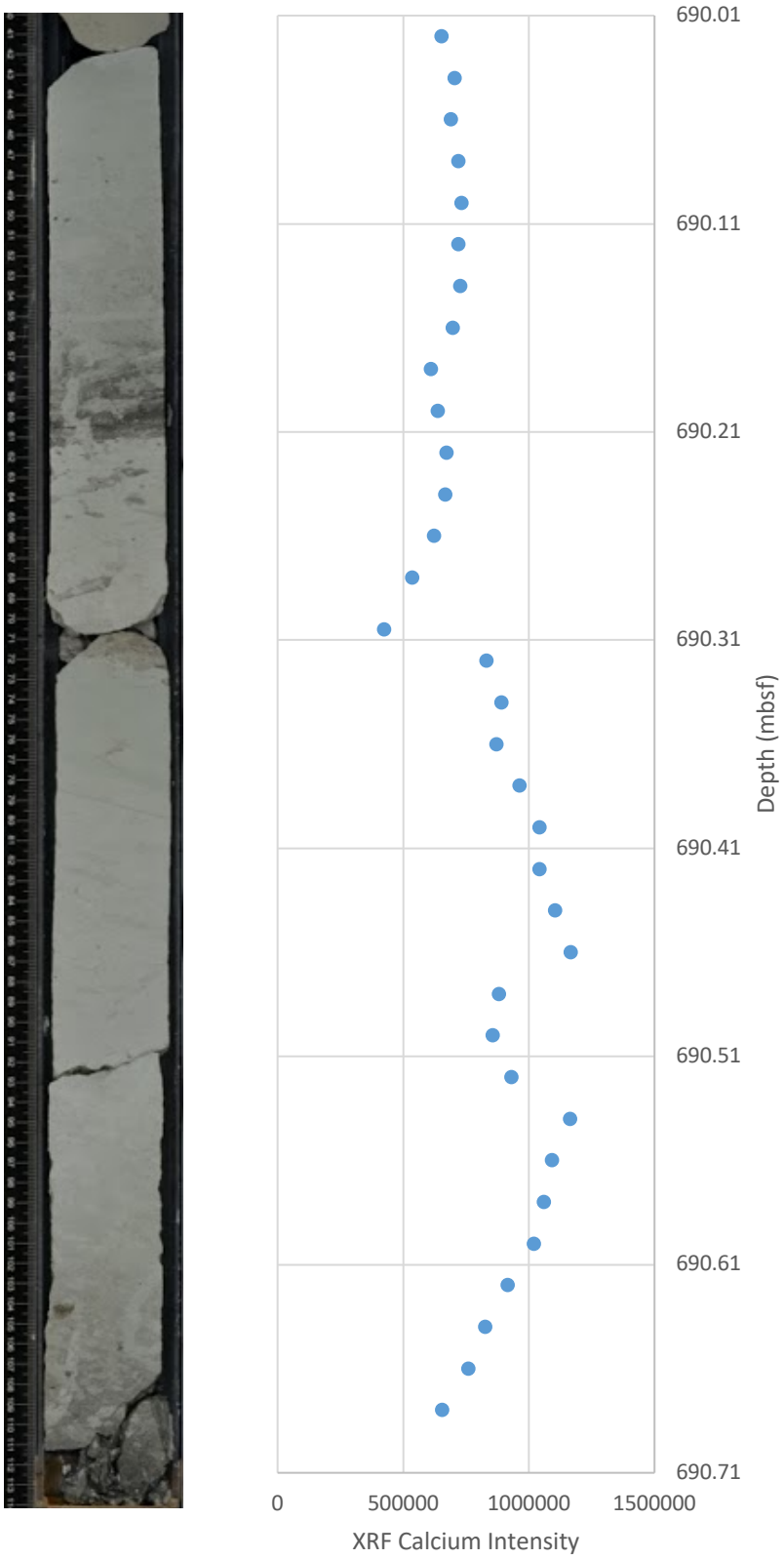

Figure A2. Representative cores image and XRF calcium intensity plotted against depth for the pelagic unit taken from core 375-U1520C-7R-1.

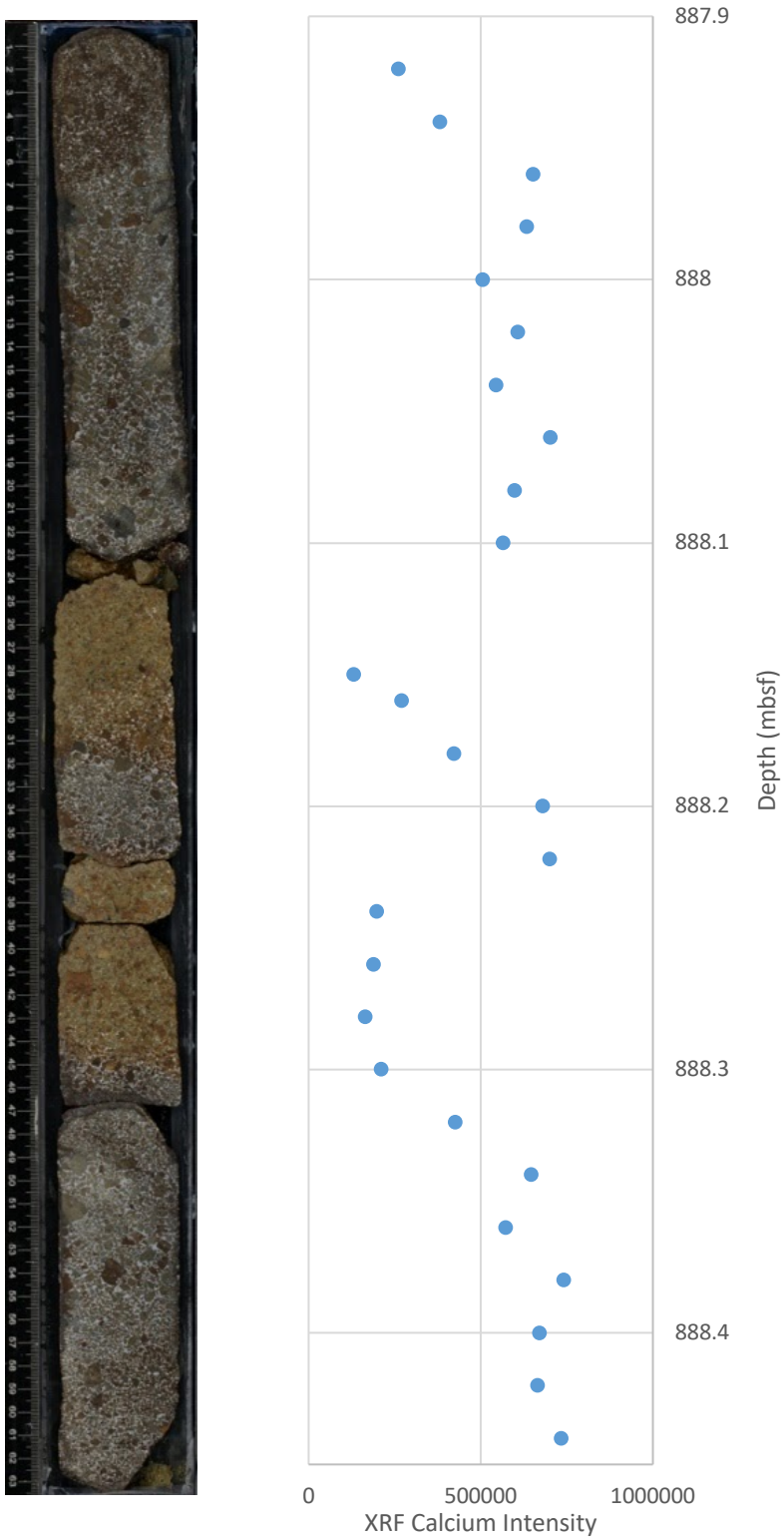

Figure A3. Representative core image and XRF calcium intensity plotted against depth for the volcaniclastic unit taken from core 375-U1520C-27R-6.

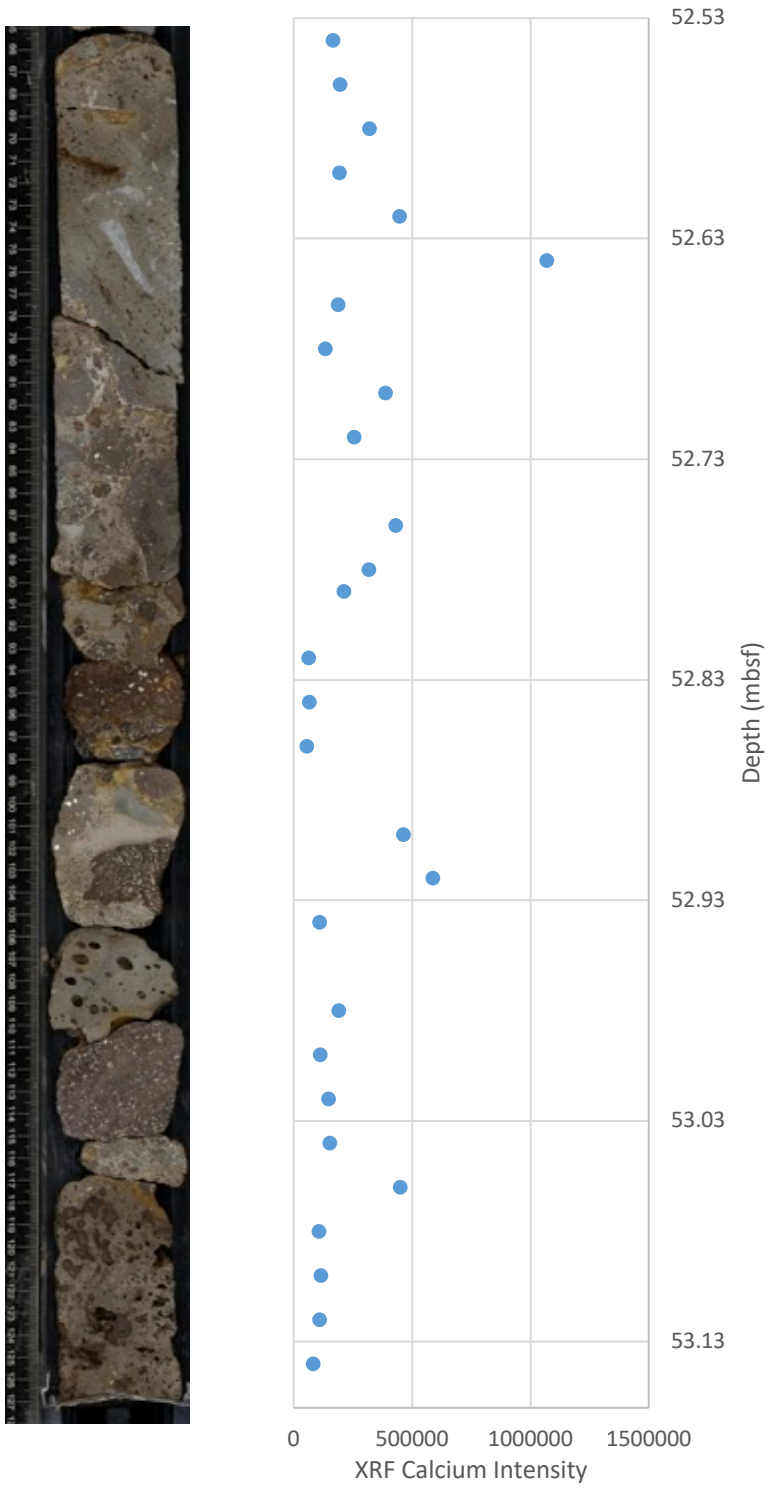

Figure A4. Representative core image and XRF calcium intensity plotted against depth for the basalt unit taken from core 375-U1526A-8R-1.